Determining the effective hydraulic properties of a highly heterogeneous soil horizon

Anatja Samouëlian, Isabelle I. Cousin, Cécile Dagès, Anthony Frison, Guy Richard

1 **Determining the effective properties of a highly heterogeneous horizon: Estimations by**

2 **numerical simulations and calculations by analytical equations**

3

4 Samouëlian A.[1,*], Cousin I.[1], Dagès C.[2], Frison A.[1], Richard G.[1]

5

6 [1]INRA, UR 0272 - Unité de Science du Sol, Centre de recherche d'Orléans, 2163 Avenue de

7 la Pomme de Pin, CS 40001 Ardon, 45075 Orléans Cedex 2, France

8 [2]INRA, UMR LISAH - Bat 24, 2 place Viala, 34060 Montpellier Cedex, France

9

10 *Corresponding author:

11 Phone: + 33 2 38 41 78 49

12 Fax: + 33 2 38 41 78 69

13 E-mail: Anatja.Samouelian@orleans.inra.fr

14

17 **Abstract**

18 In this study, we have attempted to determine the effective hydraulic properties of a highly

19 heterogeneous soil horizon composed of two elementary pedological volumes (EPVs). Our

20 upscaling approach was guided by the scaleway approach introduced by Vogel and Roth

21 (2003), in which the properties of a complex system can be estimated by multiple discrete

22 upscaling steps. This approach was tested on a dataset from laboratory measurements of

23 hydraulic conductivity at EPV scale, while explicit 3D soil structure was considered at

24 horizon scale. We then formulated a decision tree to guide the user to choose the appropriate

25 upscaling method to determine effective hydraulic conductivity at horizon scale. In the case of

26 low contrast between hydraulic conductivities at EPV scale, the effective hydraulic

27 conductivity at horizon scale can be achieved by calculating the Wiener bounds, which

28 requires only the proportion of the different EPVs. In the case of high contrast between

29 hydraulic conductivities at EPVs scale, we recommend either calculating the Cardwell and

30 Parson bounds, or performing a direct 3D numerical simulation to solve Richard's equation,

31 which requires an explicit representation of the 3D structure of the soil horizon. The Cardwell

32 and Parsons bounds remain a good and easily available approximation. Otherwise, more

33 accurate estimation can be obtained by numerical simulation though this is time-consuming.

34 A decision map is proposed to help choosing the best method for estimating effective

35 hydraulic conductivity.

36

1. Introduction

Hydraulic properties are often key parameters in environmental simulations and it is usually necessary to obtain them at horizon scale. In this context, soil horizons represent the reference soil volume in terms of soil functioning. Nevertheless, in many cases soil horizons are heterogeneous, for example, in stony horizons (Cousin et al., 2003), cultivated horizons (Richard et al., 2001), and also specific weathering horizons like those in Albeluvisols (Diab et al., 1988; Frison et al., 2009). In these cases, the determination of hydraulic properties remains difficult. Consequently, two possibilities are offered. The soil horizon can be described either by an explicit structure with distinctive hydraulic properties, or by effective soil hydraulic parameters. The first possibility requires 2D or, even better, 3D modeling, though the latter is not always practical to carry out. The second possibility is based on the assumption that the soil horizon can be represented by a homogeneous structure if it is possible to take into account the hydraulic properties at a lower scale. Nevertheless, the determination of effective hydraulic properties in heterogeneous horizons cannot be done by classical laboratory experiments on decimetric samples, such as the Multi-Step-Outflow (van Dam et al., 1994) or the Wind evaporation experiment (Wind, 1968). According to the WRB (1998), these heterogeneous horizons can be described as a combination of different elementary soil pedological volumes that have different chemical and mineralogical compositions and physical properties. For example, in the case of an Albeluvisol we can distinguish ochre and pale volumes resulting from soil evolution; in the case of a cultivated horizon, compacted and uncompacted soil clods result from mechanical stress. Here, we propose to determine the effective properties at the horizon scale based on the scaleway upscaling approach introduced by Vogel and Roth (2003). In this upscaling approach, spatial variability is considered to exist at multiple scales, and the system can be divided into multiple discrete upscaling steps. Indeed, this approach permits dealing with multiscale

62 heterogeneities without making assumptions about the heterogeneities of the underlying

63 structure, because the latter is taken into account explicitly.

64 The aim of this paper is threefold: i) to determine the hydraulic properties at the scale of the

65 soil's elementary volume, ii) to discuss benefits and disadvantages of the different analytical

66 methods for upscaling, and iii) to compare these methods with the estimation of the effective

67 hydraulic conductivity by using a direct 3D numerical simulation.

68 First, the determination of the hydraulic properties at the elementary scale of soil pedological

69 volumes is done by adapting the method proposed by Meadows et al. (2005). The second step

70 consists in developing different strategies to determine the effective hydraulic properties at

71 horizon scale. Renard and de Marsily (1997) discussed of different analytical methods based

72 on the simple calculation of bounds to estimate the effective hydraulic conductivity in

73 heterogeneous porous media. Until now, these methods have mostly been used in petroleum

74 engineering and in hydrogeology. Moreover, recent research to determine the effective

75 hydraulic properties of soil has often neglected natural soils and opted for simulated structures

76 (Knudby et al., 2006; Samouëlian et al., 2007; Durner et al., 2008). Here, we propose to apply

77 the analytical methods put forward by Renard and de Marsily (1997) in the context of Soil

78 Science, to natural soil heterogeneities and real data measurements of hydraulic properties at

79 local scale. To achieve this, we use an explicit representation of 3D soil structure measured by

80 electrical resistivity tomography (Frison 2008). We also test the accuracy of analytical

81 characteristics which can be easily computed once the structure of hydraulic properties is

82 known.

83   **2. Material and Methods**

84   2.1 Soil characteristics and structure

85   The soil studied was an Albeluvisol that exhibited several horizons composed by the

86   juxtaposition of two Elementary Pedological Volumes (EPVs). Here, we have focused on the

87   E&BT horizon, from 30 to 55 cm depth. The EPVs in this horizon can be visually

88   distinguished by their colours (ochre and pale). Their chemical and mineralogical

89   compositions (Montagne et al., 2008) and their different modes of hydraulic functioning

90   (Frison et al., 2009) were analysed on clods of the two types of EPVs, each clod being large

91   enough to be a Representative Elementary Volume of the EPV. This is consistent with

92   previous studies on E&Bt horizons (Diab et al., 1988; Wopereis et al., 1993). The pale EPVs

93   contained more silt whereas the ochre EPVs contained more clay (Table 1), but the proportion

94   of clay increased with depth inside the whole sample volume whatever the EPV. The bulk

95   density of the EPVs was around 1.5 g.cm^{-3} and was not significantly different between the

96   two types of EPV (Table 2). Further works conducted by Frison (2008) provided the 3D

97   structure of the soil horizon, and the proportion of each EPV. The characterisation of this

98   E&Bt horizon was done during autumn 2006, when no macropore was observed in the field.

99   As a consequence, only two types of EPVs, ochre EPV and pale EPV, represent the structure

100   of the horizon. The 3D structure of this heterogeneous horizon was obtained by electrical

101   resistivity measurements (fig. 1). A 3D soil block (90 cm x 52 cm x 30 cm) with the explicit

102   localisation of the ochre and pale EPVs was obtained after a simple binary threshold of the

103   electrical resistivity data. The threshold was chosen by comparison between the binary

104   resistivity image of the top of the horizon and its picture from photography (Frison, 2008).

105   Moreover, the proportion of each EPV type was calculated on this soil block: 57% for the

106   ochre EPVs and 43 % for the pale EPVs respectively.

107

108   2.2. Determining hydraulic properties at EPV scale

109   To calculate the effective hydraulic properties at horizon scale, experiments were first

110   conducted at EPV scale. Large undisturbed blocks of the E&BT horizon – about 10,000 cm^3-

111   were sampled when the soil was near field capacity during the autumn season. They were

112   carefully stored at 4°C to avoid both structural disturbance by biological activity and loss of

113   water. Before the experiments, each soil block was gently cut by hand, to separate the ochre

114   EPVs and the pale EPVs, without destroying their structure. Each EPV was roughly

115   cylindrical, with a diameter of at least 2 cm and a height of about 4 cm.

116   To keep the soil sample intact and avoid destruction during the experiments, the EPVs were

117   embedded in paraffin wax and then placed in small plastic cylinders (6 cm in diameter, 6 cm

118   in height).

119   Saturated hydraulic conductivity was determined with the constant-head method (Stolte,

120   1992) by using a mini-permeameter whose diameter was equal to the diameter of the plastic

121   cylinder. After this experiment, the method proposed by Meadows et al. (2005) was adapted.

122   The cylinder was placed on a mass balance and a mini tensiometer was inserted horizontally

123   at the centre of the saturated EPV and equipped with a pressure transducer to continuously

124   measure soil water potential. From these experimental data, the water retention curve and the

125   unsaturated hydraulic conductivity were estimated by inverse modelling using HYDRUS-1D

126   (Simunek et al., 2005). The water retention curve was parameterized by the modified van

127   Genuchten equation with an air-entry value equal to -2 cm, and the unsaturated hydraulic

128   conductivity was parameterized by the Mualem-van Genuchten equation (Mualem, 1976; van

129   Genuchten, 1980):

130    $\theta = \theta_{sat}$ if $h \geq$ - 2 cm

131    $\dfrac{\theta - \theta_r}{\theta_s - \theta_r} = \left[1 + (\alpha|h|)^n\right]^{-(1-1/n)}$ if $h <$ - 2 cm   [1]

132
$$K(Se) = K_0 \qquad\qquad \text{if } h \geq -2 \text{ cm}$$

133
$$K(Se) = K_0 Se^{l}\left[1 - \left(1 - Se^{1/m}\right)^{m}\right]^{2} \qquad \text{if } h < -2 \text{ cm} \qquad\qquad [2]$$

134
with $Se = \dfrac{\theta - \theta_r}{\theta_s - \theta_r}$ $\qquad\qquad\qquad\qquad\qquad\qquad\qquad$ [3]

135   where h is the water potential (m), θ the volumetric water content ($m^3 m^{-3}$), θ_s the saturated

136   water content ($m^3 m^{-3}$), θ_r the residual water content ($m^3 m^{-3}$), l the tortuosity factor, here taken

137   as equal to 0.5, K_0 ($m.s^{-1}$) the hydraulic conductivity at $h = 0$, m, and n and α (m^{-1}) are fitting

138   parameters.

139   We chose the following conditions for the inversion:

140   Boundary conditions: no flux occurred at the lower EPV boundary while the flux at the

141   surface of the EPV was recorded during the experiment and corresponded to the loss of mass

142   of the whole sample, i.e. the loss of water through evaporation.

143   Initial condition: a linear distribution of water potential with depth was used.

144   The objective function of the inverse problem was defined with both the values of the water

145   potential recorded in the middle of the sample by the microtensiometer, and the values of the

146   water content calculated from the loss of mass recorded by the mass balance. Among the

147   parameters to be determined, two of them were fixed before the inversion: parameter K_0 was

148   taken as equal to the measured value ($K_0 = K_{sat}$) with K_{sat} being the saturated hydraulic

149   conductivity; parameter θ_s was taken as being equal to the porosity and estimated with the

150   EPV mass and the EPV volume, assuming a particle density equal to 2.65 g cm^{-3}. Quality of

151   the fit was check through the mass balance error.

152

153   2.3. Determination of effective hydraulic properties

154

155   *2.3.1 Case studies*

156   Three case studies were analysed from the results at EPV scale: case 1: the highest contrast

157   between the hydraulic properties of the ochre and pale EPVs was taken into account; case 2:

158   the mean value of the hydraulic properties calculated for each type of EPV was taken into

159   account; and case 3: the lowest contrast of hydraulic properties between the ochre and the pale

160   EPVs was taken into account.

161

162   *2.3.2 Effective water retention curve*

163   The effective water retention curve was obtained from the additive properties of the water

164   retention curves at local scale, introduced by Durner (1994). This was achieved by an

165   expansion of the modified van Genuchten parametrization to a k-modal form (Vogel et al.,

166   2008):

167
$$S_e(h) = \sum_{i=1}^{k} \omega_i \left[(1 + \alpha_i h)^{n_i} \right]^{-1 + 1/n_i} \qquad [4]$$

168   where $S_e(h)$ is the effective water saturation. The relative weight of the different modes ω_i

169   fulfilled the condition $\sum_i \omega_i = 1$ while n_i and α_i are the related van Genuchten parameters (van

170   Genuchten, 1980). In our study, ω, the volume proportion of the different EPVs was equal to

171   0.43 for the pale EPVs and to 0.57 for the ochre EPVs.

172

173   *2.3.3 Effective hydraulic conductivity*

174   The effective hydraulic conductivity was determined with two different methods: numerical

175   3D variably saturated flow modeling, and an analytical method with the calculation of

176   mathematical bounds. It should be noted that the analytical method consisted in fast and easy

177   calculation, compared to the numerical one that requires a numerical 3D code to solve

178   Richards equation.

179

180   2.3.3.1 Numerical simulation of the effective hydraulic conductivity calculation

181   The effective hydraulic conductivity $K_{eff}(h)$ of the E&Bt horizon was obtained by solving

182   Richards equation using Hydrus 3D (Simunek et al., 07). The 3D soil structure at horizon

183   scale (fig. 1) was used to allocate each node (15 600 in total) of the finite element mesh to

184   ochre or pale soil hydraulic properties. We used a modified hexahedral mesh with 80 850

185   elements to spatially describe the soil horizon. The average size of each element was about 2

186   cm^3, whereas the sizes of the pale and ochre EPVs ranged from some centimeters to

187   decimeters.

188   Numerical simulations were the same as described by Samouëlian et al. (2007). A steady-state

189   flow regime was simulated by applying a constant water potential h at the upper and the lower

190   boundary, so that gravity was the only driving force and the soil potential was approximately

191   constant throughout the domain. The initial condition was a constant pressure head, whereas

192   the vertical boundaries were considered as no-flux boundaries since the flow was assumed to

193   be mainly vertical. This calculation was done for 102 pressures starting from saturated (h =

194   0hPa) to unsaturated conditions (h = -10000hPa). For each water potential value, the

195   simulation time was chosen so that the steady-state flow condition was reached. The highest

196   mass balance error that was accepted was 0.003%. Finally, we obtained $K_{eff}(h)$ which is

197   equal to the simulated flux.

198

199   2.3.3.2 Calculation of the analytical bounds

200   Three types of analytical bounds, namely those of Wiener (1912), Matheron (1967), Cardwell

201   and Parsons (1945), were calculated to estimate the hydraulic conductivity of the

202   heterogeneous E&Bt soil horizon.

203   The calculation of the Wiener and Matheron bounds is based on an assumption of the spatial

204   arrangement of the different EPVs constituting the soil horizon and takes into account their

205 proportion. The Wiener bounds assumed a layered model structure. When the flux is parallel

206 to the main direction of organization of the two types of EPVs, the effective conductivity at

207 each water potential, $m_a(h)$, is given by the arithmetic mean of the hydraulic conductivity of

208 each EPV:

209
$$m_a(h) = \sum_{i=1}^{2} \omega_i K_i(h) \qquad [5]$$

210 where ω_i represents the volume proportion of each EPV and $K_i(h)$ represents the hydraulic

211 conductivity of EPV i at water potential h.

212 When the flux is perpendicular to the main direction of organization of the two types of

213 EPVs, the effective conductivity at each water potential, $m_h(h)$, is given by the harmonic

214 mean of the hydraulic conductivity of each EPV:

215
$$1/m_h(h) = \sum_{i=1}^{2} \omega_i / K_i(h) \qquad [6]$$

216 In a more complex arrangement of the different types of EPV, the effective hydraulic

217 conductivity of the E&BT horizon $K_{eff}(h)$ is comprised between these two theoretical bounds:

218
$$m_h(h) \le K_{eff}(h) \le m_a(h) \qquad [7]$$

219 In the calculation of the Matheron bound, we consider that the geometry of the porous

220 medium is isotropic. In this case the effective hydraulic conductivity $K_{eff}(h)$ is equal to:

221
$$K_{eff}(h) = m_a(h)^{\alpha} m_h(h)^{1-\alpha} \quad \text{with } \alpha = (D-1)/D \qquad [8]$$

222 where D is the spatial dimension.

223 Cardwell and Parsons (1945) proposed to take account of the spatial 3D arrangement of the

224 soil horizon to define the upper and lower bounds. The effective conductivity in a given

225 direction is bounded by: 1) the arithmetic mean of the harmonic means calculated on each cell

226 line parallel to the main flow direction (lower bound); 2) the harmonic mean of the arithmetic

227 means on each slice of a cell perpendicular to the main flow direction (upper bound). If the

228   main flow is orientated along the vertical z axis, the effective conductivity $K_{eff}(h)$ is then

229   bounded by:

230
$$m_a^x(h)\left[m_a^y(h)\left(m_h^z(h)\right)\right] \le K_{eff}(h) \le m_h^z(h)\left[m_a^y(h)\left(m_a^x(h)\right)\right]$$
[9]

231 **3. Results**

232 3.1. Water retention curves of each pair of EPVs and the effective water retention curve at

233 horizon scale

234 *3.1.1 Comparison of the water retention curve for the pale and ochre EPVs*

235 Figure 2a presents the water retention curve estimated from evaporation experiments for 17

236 pale and ochre EPVs. For potentials higher than about -1000 hPa, the volumetric water

237 content was generally higher in the pale EPVs than in the ochre ones, which was in agreement

238 with higher porosity due to biological structures (earthworm and plant roots) observed in the

239 field in the pale EPVs. On the contrary, for water potentials lower than -1000 hPa, the water

240 content was higher in the ochre EPVs, due to their higher clay content (Table 1) (Montagne et

241 al., 2008; Frison et al., 2009). Nevertheless, the variability in the water retention curve within

242 the different EPVs was high. Statistical tests on water content for water potentials equal to -10

243 hPa, - 33 hPa, -100 hPa, -330 hPa, -500 hPa and -1000 hPa showed that the difference in

244 water content between the two types of EPV was significant for water potentials equal to or

245 higher than -100 hPa and non significant for water potentials equal to or lower than -330 hPa.

246 The hydraulic parameters of the three cases are summarized in Table 3.

247

248 *3.1.2 Calculation of the effective water retention curve at horizon scale*

249 According to equation [4], the effective water retention curve at the horizon scale must be

250 localized inside the domain defined by the water retention curves of the pale and ochre EPVs.

251 Because the proportion of ochre EPVs was slightly higher (57%) compared to the pale EPVs

252 (43%), the resulting effective water retention curve was closer to the ochre EPV water

253 retention curve. Figure 2b presents the results for case 1; nevertheless the tendency was the

254 same for the other cases 1 and 2, but the amplitude of the contrast between the water retention

255 curves at EPV scale became decreasingly significant (results not shown here).

256 3.2. Hydraulic conductivity of each pair of EPVs and determination of effective hydraulic

257 conductivity

258 *3.2.1 Comparison of the hydraulic conductivity curve for the pale and ochre EPVs*

259 Figure 3a presents the hydraulic conductivity curve for 8 pale and 9 ochre EPVs. Statistical

260 tests performed on the logarithmic value of hydraulic conductivity for water potentials equal

261 to those already studied for the water retention curve, i.e. -10 hPa, - 33 hPa, -100 hPa, -330

262 hPa, -500 hPa and -1000 hPa, showed that hydraulic conductivity was always significantly

263 different for the pale EPVs and for the ochre EPVs: hydraulic conductivity was higher in the

264 pale EPVs whatever the water potential.

265 As shown in figure 3b, the contrast in hydraulic conductivity between ochre and pale EPVs

266 was different for the three cases. The difference in hydraulic conductivity between pale and

267 ochre EPVs was maximal for a water potential around -1000 hPa for case 1, and around -400

268 hPa for case 2. For more negative water potentials, the difference decreased slightly.

269 Concerning case 3, the difference in hydraulic conductivity between the ochre and pale EPVs

270 was negligible. To check this difference, we also calculated the surface area, defined by

271 integral differences, between the two hydraulic conductivity curves for each case (fig. 4). As

272 seen in Table 4, this surface area varied by one order of magnitude between case 1 and case 3.

273

274 *3.2.2 Calculation of the effective hydraulic conductivity curve at horizon scale*

275 The estimation of the effective hydraulic conductivity curve by the numerical simulation was

276 assumed to be the closest to the real hydraulic conductivity and was thus considered as the

277 reference hydraulic conductivity curve. As expected, whatever the case, it was between the

278 hydraulic conductivity curves of each EPV, and was closer to the hydraulic conductivity of

279 the pale EPVs (fig. 4), although the proportion of ochre EPVs was higher. This example backs

280 up the argument that hydraulic conductivity is above all correlated to the soil structure.

281   For case 3 (fig. 4c), the effective hydraulic conductivity curves estimated by the numerical

282   simulation and calculated by the analytical bounds merged as the contrast in hydraulic

283   conductivity was low. Contrary to case 3, cases 1 and 2 presented distinct effective hydraulic

284   conductivity curves. As seen in figure 4a and 4b, the Wiener bounds and the Cardwell &

285   Parsons bounds delineated a surface area inside the domain of the hydraulic conductivity

286   curves of the ochre and pale EPVs. These domains included the effective hydraulic

287   conductivity curve estimated by the numerical simulation. By definition the Cardwell &

288   Parsons domain is included inside the Wiener domain. Indeed the heterogeneous structure is

289   taken into account by the Cardwell & Parsons bounds. The Wiener bounds assume an extreme

290   geometric structure of soil with a layered structure. This is in agreement with calculation of

291   the surface areas of the two domains: $S_{Wiener} \geq S_{Cardwell-Parsons}$, whatever the case (Table 4).

292   The results of our study showed that the high Wiener bound (calculation of the arithmetic

293   mean) was closer to the numerical simulation than the low Wiener bound (calculation of the

294   harmonic mean). This means that the general structure of the E&BT horizon was more or less

295   parallel to the water flow. This was consistent with field observations of vertical tongues of

296   pale EPVs and image analysis observations (Cornu et al., 2007).

297

4. Discussion

299   As shown previously, for the estimation of the effective hydraulic conductivity at horizon

300   scale, different situations could occur, depending on the contrast of the hydraulic conductivity

301   of each elementary EPV. Here, we propose a decision tree to guide the user in choosing the

302   method best-adapted for estimating the effective hydraulic conductivity of a heterogeneous

303   soil horizon (fig. 5). First of all, for any anisotropic medium like soil, the structure must be

304   studied roughly, for example, by qualitative soil profile observation. The two extreme cases

305   consist in a layered porous medium, where the elementary pedological volumes would be

306   either parallel or perpendicular to the water flow. Between these two extreme structures,

307   various possibilities of structure topology and connectivity can be considered, as is often the

308   case for the natural soil horizon. Indeed, recent research has pointed out that the topology of

309   the sub-scale structure may be of crucial importance for upscaling hydraulic conductivity

310   (Western et al., 2001; Zinn and Harvey, 2003; Knudby et al., 2006; Samouëlian et al., 2007).

311   Here, we propose to take into account not only the topology but also the contrast between the

312   hydraulic conductivity curves at EPV scale to choose the appropriate upscaling method: either

313   estimation by numerical simulation or calculation using the analytical bounds.

314   i)   When the contrast between the hydraulic conductivity curves of the two types of

315   EPV is low, the effective hydraulic conductivity can be rapidly and easily

316   estimated by the calculation of the domain defined by the Wiener bounds. This

317   method requires only the volume proportion of the different EPVs.

318   ii)   When the contrast between the hydraulic conductivity curves of the two types of

319   EPV is high, we recommend either estimating the effective hydraulic conductivity

320   by numerical simulation, or calculating it with Cardwell-Parsons bounds. Both

321   methods require the 3D structure of the soil horizon. An initial estimation could be

322   given quickly by the calculation of the Cardwell and Parsons bounds. Depending

323   on the required accuracy, this first estimation can be sufficient. Otherwise, a more

324   accurate estimation can be provided by numerical simulation. Nevertheless, it

325   should be noted that this numerical simulation is much more time consuming than

326   the calculation of analytical bounds.

327   Nevertheless, determining an absolute value for a "high" or a "low" contrast of hydraulic

328   conductivity at EPV scale remains difficult. One way of deciding whether Wiener bounds can

329   be used consists in calculating their ratio, which itself depends on the ratio between the

330   hydraulic conductivity curves of the two types of EPV and the volume percentage of each

331   EPV. This ratio R_W is equal to:

332
$$R_W = \frac{\left[\omega_p \dfrac{K_p(h)}{K_o(h)} + (1-\omega_p)\right]\left[\omega_p + (1-\omega_p)\dfrac{K_p(h)}{K_o(h)}\right]}{\dfrac{K_p(h)}{K_o(h)}} \qquad [10]$$

333   where $K_p(h)$ and ($K_o(h)$) represents the hydraulic conductivity of the pale EPVs the ochre

334   EPVs respectively, while ω_p is the volume fraction of the pale EPV. When the contrast

335   between the hydraulic conductivity curves is low, the R_W ratio between the two Wiener

336   bounds is close to one. This means that the Wiener bounds enclose a rather narrow region in

337   which the actual effective hydraulic conductivity is located. For more complex cases, we

338   propose a decision map based on the R_W ratio, in order to simultaneously track the effect due

339   to the contrast between hydraulic conductivity at EPV scale, and that for each possible

340   proportion between the two EPVs. The hydraulic conductivity contrast was extended up to 4.5

341   in log scale, covering by this way the range of hydraulic properties proposed by Vogel et al.,

342   (2006) between macropores and a soil horizon. In our study, we consider that the Wiener

343   bounds could be correctly applied when the R_w value is lower than 3 (fig. 6). Nevertheless the

344   R_w threshold value has to be considered case to case by the user, depending i) on the accuracy

345   of the measurements themselves at the lower scale, and ii) on the expected accuracy required

346   for the simulation. In our survey, the cases 1 and 2 have R_w ratios lower than 3 and the use of

347   Wiener bounds remained then acceptable. Consequently, by calculating effective hydraulic

348   conductivity it is possible to avoid the difficulties related to numerical simulation. For case 3,

349   the R_W ratios were from around 3 to 100; the contrast between the hydraulic conductivity

350   curves of the pale and ochre EPVs therefore remained too high (around 2.5 in log scale) to

351   estimate the effective hydraulic conductivity by using the Wiener domain. In this case, the

352   calculation of the effective hydraulic conductivity curve by the Cardwell and Parsons bounds

353   remained the best and most easily available approximation.

354

355   This decision tree was built with the assumption that the structure was bimodal at horizon

356   scale. Nevertheless, according to the scaleway upscaling approach introduced by Vogel and

357   Roth (2003), the applied concept could be generalized to estimate effective hydraulic

358   conductivity at scale n from knowledge of scale n-1. With respect to Wiener bounds assuming

359   a layered structure this suggest a simple way for upscaling to the scale of soil profiles or even

360   watershed. Nevertheless, this approach only allows the calculation of the vertical flux

361   component, so that this concept would be valid only when lateral flows are negligible or else

362   can be neglected.

363   At profile scale, the general structure of the soil is layered, with horizons sub-parallel to the

364   soil surface and generally perpendicular to the main water flow. Consequently, an easy way to

365   estimate the effective hydraulic properties at profile scale would be to calculate the low

366   Wiener bound, that is to say the harmonic mean of the hydraulic conductivity of the different

367   superimposed soil horizons weighted by their thickness (fig. 5).

368   At small watershed scale, it can be assumed that the general organization of the pedological

369   mantel consists of a juxtaposition of soil units. If we hypothesize that the general

370   hydrodynamic functioning of this watershed is vertical, and that the hydraulic conductivity

371   curve of each soil unit is known, we can calculate the effective hydraulic conductivity curve

372   of the watershed from the high Wiener bound, that is to say the arithmetic mean weighted by

373   the surface area of each soil unit.

374   **5. Conclusion**

375   In this study we investigated the impact of using different analytical bounds to upscale the

376   effective hydraulic properties of a complex horizon, and especially hydraulic conductivity.

377   The calculations of the analytical bounds were either based on the volume proportion of the

378   different EPVs (Wiener and Matheron), or on the 3D structure (Cardwell and Parson), which

379   included additional topological and connectivity information about soil structure. As already

380   acknowledged in the literature, prior knowledge of topology and connectivity leads to more

381   precise determination of effective hydraulic conductivity. However, because calculating

382   analytical bounds is much easier than performing a numerical simulation based on a 3D

383   structure, we defined the case in which the first method would lead to satisfactory results. We

384   demonstrated that the contrast of hydraulic conductivity between the two EPVs was crucially

385   important for choosing the most appropriate method to estimate effective hydraulic

386   conductivity. Indeed, for a low contrast between these two EPVs, it was shown that the

387   Wiener method, which requires only the volume proportions of each EPV, provided

388   satisfactory results. For high contrast between the two EPVs, an adequate upscaling method

389   required the 3D soil structure, i.e. topology and connectivity. For a hydraulic contrast equal or

390   higher than the case 3, the use of Wiener bounds is then inadvisable. The calculation using

391   Cardwell and Parson bounds is recommended at first because it is simpler to compute. If the

392   accuracy of the calculated effective hydraulic conductivity is not sufficient, the numerical

393   simulation is then the most relevant method.

394   We then used our results to propose a decision map that can be used for other studies to help

395   choosing the appropriate analytical bounds as a function of the accuracy expected up to a

396   conductivity contrast of 4.5 in log scale.

397   Our results are based on a natural soil horizon defined by only two EPVs, but extrapolation to

398   more than two EPVs is easy. The sole restriction is the need to define the hydraulic properties

399 at EPV scale. Moreover this approach was tested on real measurements at EPVs scale

400 combined with an explicit 3D structure at horizon scale, but it can be generalized for

401 estimating effective hydraulic conductivity at other scales. For example, this approach could

402 be applied to define effective soil hydraulic properties for each soil unit at watershed scale,

403 leading to better account being taken of heterogeneous soil horizons in simulations of

404 environmental functioning.

405

408

5. References

409 Cardwell, W.T. and Parsons, R.L. 1945. Average permeabilities of heterogeneous oil sands. Trans.

411 Am. Inst. Mining. Met. Pet. Eng: 34-43.

412 Cornu, S. Montagne, D., Maguin, F., Le lay, C., Chevallier, P. and Cousin, I. 2007. Influence of

413 human impacts on Albeluvisol analysed by X-ray microfluorescence: Relative evolution of the

414 transforming front at the tongue scale. Science of the Total Environment, 377(2-3): 244-254.

415 Cousin, I., Nicoullaud, B. and Coutadeur, C. 2003. Influence of rock fragments on the water retention

416 and water percolation in a calcareous soil. Catena, 53(2): 97-114.

417 Diab, M., Merot, P. and Curmi, P. 1988. Water-Movement in a Glossaqualf as measured by two

418 tracers. Geoderma, 43(2-3): 143-161.

419 Durner, W. 1994. Hydraulic conductivity estimation for soils with heterogeneous pore structure. Water

420 Resources Research, 30(2): 211-223.

421 Durner, W., Jansen, U. and Iden, C. 2008. Effective hydraulic properties of layered soils at the

422 lysimeter scale determined by inverse modeling. European Journal of Soil Science, 59, 114-124.

423 Frison, A., Cousin, I., Montagne, D. and Cornu, S. 2009. Soil hydraulic properties in relation to local

424 rapid soil changes induced by field drainage: a case study. European Journal of Soil Science,

425 60(4): 662-670.

426 Frison, A. 2008 Analyse et modélisation des propriétes hydriques d'un horizon hétérogène de sol.

427 Thèse de l'Université d'Orléans, 228 p.

428 Knudby, C., Carrera, J., Bumgardner, J.D. and Fogg, G.E. 2006. Binary upscaling - the role of

429 connectivity and a new formula. Advances in Water Resources, 29: 590-604.

430 Matheron, G., 1967. Eléments pour une théorie des milieux poreux, Paris.

431 Meadows, D., Young, M.H. and McDonnald, E. 2005. A laboratory method for determing the

432 unsaturated hydraulic properties of soil peds. Soil Science Society of America Journal, 69: 807-

433 815.

434 Montagne, D. Cornu, S., Josiére, O., Le Forestier, L., Daroussin, J. and Cousin, I. 2008. Soil drainage

435 as a factor of human-induced soil evolution: quantification of such an evolution in an

436 Albéluvisol. Geoderma, 145(3-4): 426-438.

437   Mualem, Y. 1976. A new model for predicting the hydraulic conductivity of unsaturated porous

438   media. Water Resources Research, 12: 513-519

439   Renard, Ph. and de Marsily, G. 1997. Calculating equivalent permeability: A review. Advances in

440   Water Resources, 20(5-6): 253-278.

441   Richard, G., Cousin, I., Sillon, J.F., Bruand, A. and Guerif, J. 2001. Effect of compaction on the

442   porosity of a silty soil: influence on unsaturated hydraulic properties. European Journal of Soil

443   Science, 52(1): 49-58.

444   Samouëlian, A., Vogel, H.J. and Ippisch O. 2007. Upscaling hydraulic conductivity on the topology of

445   the sub-scale structure. Advances in Water Resources, 30, 1179-1189.

446   Šimůnek J., Sejna M. and van Genuchten M.Th., 2007. Software package for simulating the two and

447   three dimensional movement of water, heat and multiple solutes in variably saturated media,

448   user manual, version 1.07 203 p.

449   Šimůnek, J., van Genuchten, M. Th. and Šejna, M. 2005. The HYDRUS-1D Software Package for

450   Simulating the Movement of Water, Heat, and Multiple Solutes in Variably Saturated Media,

451   Version 3.0, HYDRUS Software Series 1, Department of Environmental Sciences, University of

452   California Riverside, Riverside, California, USA, 270 pp.

453   Stolte, J. 1992. Determination of the saturated hydraulic conductivity using the constant head method.

454   Manual soil physical measurements, version 2.0. Technical Document sc-dlo, Wageningen, 4p.

455   van Genuchten, M.T. 1980. A Closed-Form Equation For Predicting The Hydraulic Conductivity of

456   Unsaturated Soils. Soil Science Society of America Journal, 44(5): 892-898.

457   Vogel, H.J., Samouëlian, A. and Ippisch, O. 2008. Multi-step and two-step experiments in

458   heterogeneous porous media to evaluate the relevance of dynamic effects. Advances in Water

459   Resources, 31:181-188.

460   Vogel H.J., Cousin I., Ippisch O., Bastian P., 2006. The dominant role of structure for solute transport

461   in soil: experimental evidence and modelling of structure and transport in a field experiment.

462   Hydrology and Earth System Sciences, 10, 495-506.

463   Vogel, H.J. and Roth, K. 2003. Moving through scales of flow and transport in soil. Journal of

464   Hydrology, 272(1-4): 95-106.

465   Western, A.W., Blöschl, G. and Grayson, R.B. 2001. Toward capturing hydrologically significant

466   connectivity in spatial patterns. Water Resources Research, 37(1): 83-97.

467   Wiener, O. 1912. Abhandlungen der Mathematisch. Physischen Klasse der königlichen sächsischen

468   Gesellschaft(32): 309.

469   Wind, G.P. 1968. Capillary conductivity data estimated by a simple method. In: E. P.E. Rijtema and

470   H. Wassink (Editor), Water in the Unsaturated Zone, Gentbrugge, Belgium, pp. 181–191.

471   Wopereis, M.C.S., Kropff, M.J., Wösten, J.H.M. and Bouma, J. 1993. Sampling strategies for

472   measurement of soil hydraulic properties to predict rice yield using simulation models.

473   Geoderma, 59: 1-20.

474   WRB, 1998. A world reference base for soil resources. In: O.C.S. J.A. Deckers, F.O. Nactergaele,

475   L.R. Oldeman, R. Brinkman (Editor), World Soil Resources, Report n°84. FAO-ISRIC-AISS,

476   Rome, Italia.

477   Zinn, B. and Harvey, C.F. 2003. When good statistical models of aquifer heterogeneity go bad: A

478   comparaison of flow, dispersion, and mass transfer in connected and multivariate hydraulic

479   conductivity fields. Water Resources Research, 39(3): 1-18.

480

481   **List of figures**

482   Figure 1: Binary 3D representation of the E&BT horizon, with ochre (orange color on the figure) and

483   pale elementary pedological volumes (light grey color on the figure) obtained after electrical

484   resistivity tomography (from Frison 2008).

485

486   Figure 2: Water retention curve of the horizon studied.

487   –a- Water retention curve determined by the evaporation method on 8 pale EPVs and 9 ochre EPVs.

488   The bold lines represent the mean curve for each type of EPV. At some water potentials, a Student t-

489   test has enabled determining if the volumetric water content was significantly different (the letters are

490   different when the water contents are significantly different).

491   -b- Effective water retention curve at horizon scale for case 1 (black line). (The ochre and grey lines

492   represent the highest contrast in water retention curves at EPV scale).

493

494   Figure 3: Unsaturated hydraulic conductivity curve at EPV scale.

495   -a- Unsaturated hydraulic conductivity curve determined by the evaporation method on 8 pale EPVs

496   and 9 ochre EPVs. The bold lines represent the mean curve for each type of EPV. At some water

497   potentials, a Student t-test has enabled determining if the volumetric water content was significantly

498   different (the letters are different when the water contents are significantly different).

499   -b- Ratio between the hydraulic conductivity curve of the pale and ochre EPVs for the three study

500   cases (case 1: square symbols; case 2: circle symbols; case 3: cross symbols).

501

502   Figure 4: Hydraulic conductivity of each EPV ochre and pale (respectively ochre and grey line), and

503   effective hydraulic conductivity after Wiener bounds (black line), Matheron bound (grey bold line),

504   Cardwell and Parsons bounds (square symbols) and numerical simulation (red line) for each case

505   study: a) case 1, b) case 2, c) case 3

506

507   Figure 5: Decision tree for effective hydraulic conductivity determination in an anisotropic medium

508   assuming vertical fluxes.

509 Figure 6: Evolution of the Wiener bounds ratio (R_W) according to the hydraulic conductivity contrast

510 of two EPVs and to the volume proportion of the EPVs. The black bar and the grey arrows represent

511 the R_W domain for the 3 cases in our study (here the ωp value is equal to 0.43).

512

513

514

515 List of tables

516

517 Table 1: Particle-size distribution of the pale and ochre EPVs in the upper and lower parts of the

518 E&BT horizon. (The particle-size distribution was determined according to the French normalized

519 protocol X 31-107).

520

521 Table 2: Bulk density at sampling and saturated water content of the pale and ochre EPVs in the upper

522 and lower parts of the E&BT horizon

523

524 Table 3: Hydraulic conductivity parameters for the pale and the ochre EPVs and for the three cases

525 studies.

526

527 Table 4: Calculated surface area: S_{EPV} between pale and ochre EPV hydraulic conductivity, S_{Wiener}

528 between Wiener bounds, $S_{Cardwell-Parsons}$ between, respectively, Cardwell and Parsons bounds, $S_{Cardwell-}$

529 $_{Parsons\_Numerical\ Simulation}$, $S_{Wiener\_Numerical\ Simulation}$ between Cardwell and Parsons upper bound, lower bound,

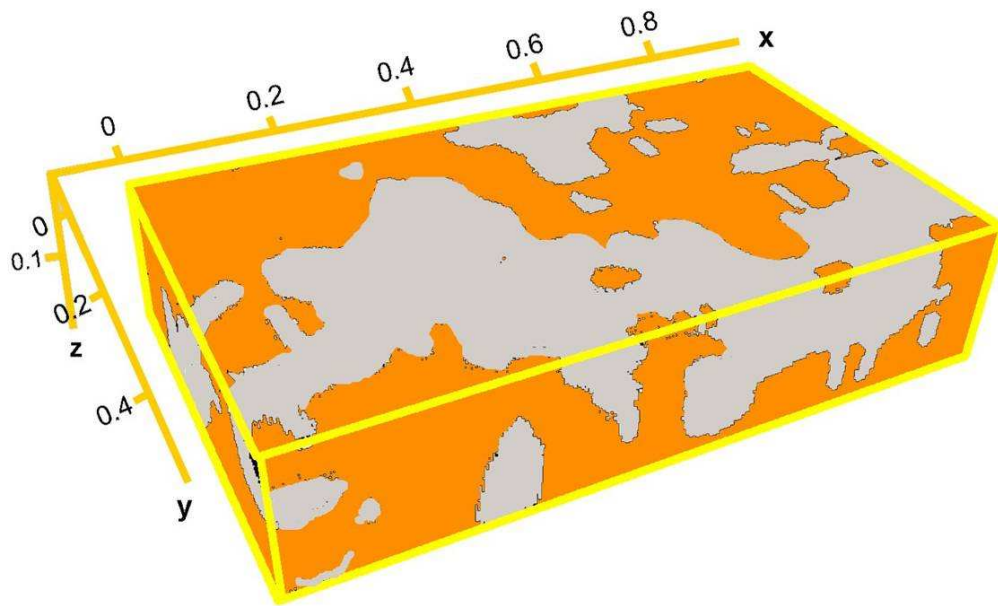530 Wiener upper bound, lower bound and effective hydraulic properties defined with the numerical

531 simulation.

532
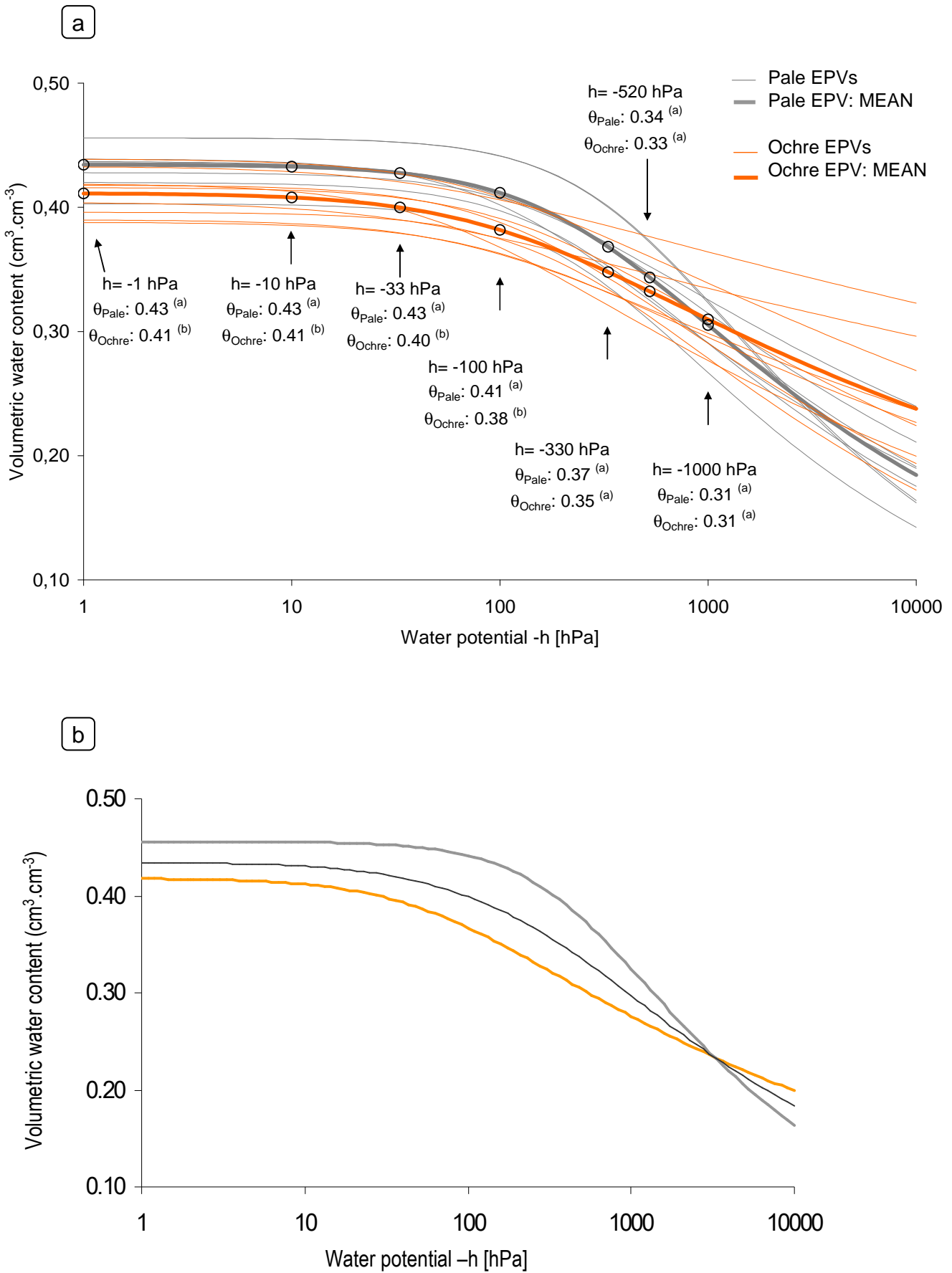
Figure 1

Figure 2

Figure 3
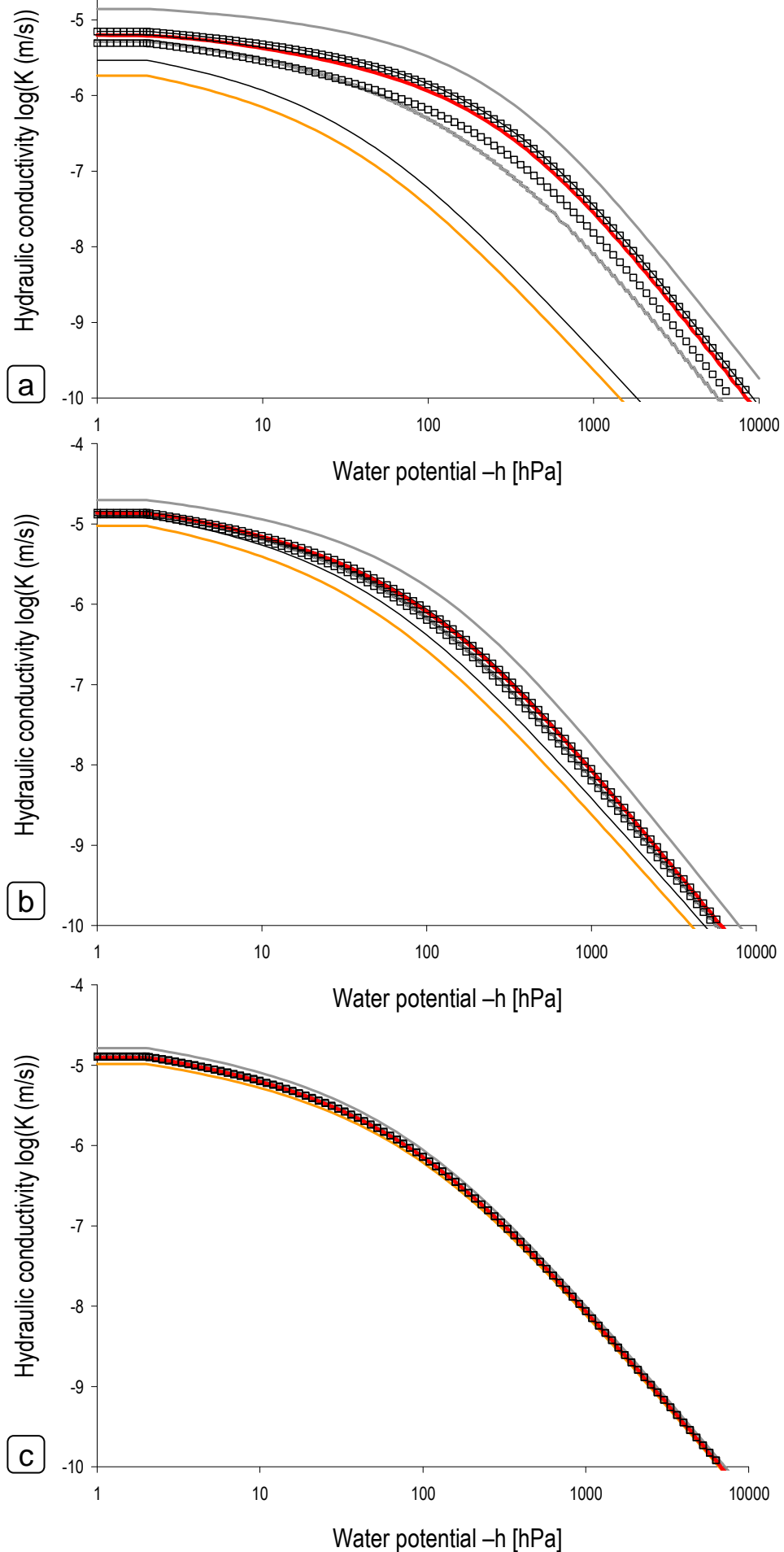
Figure 4
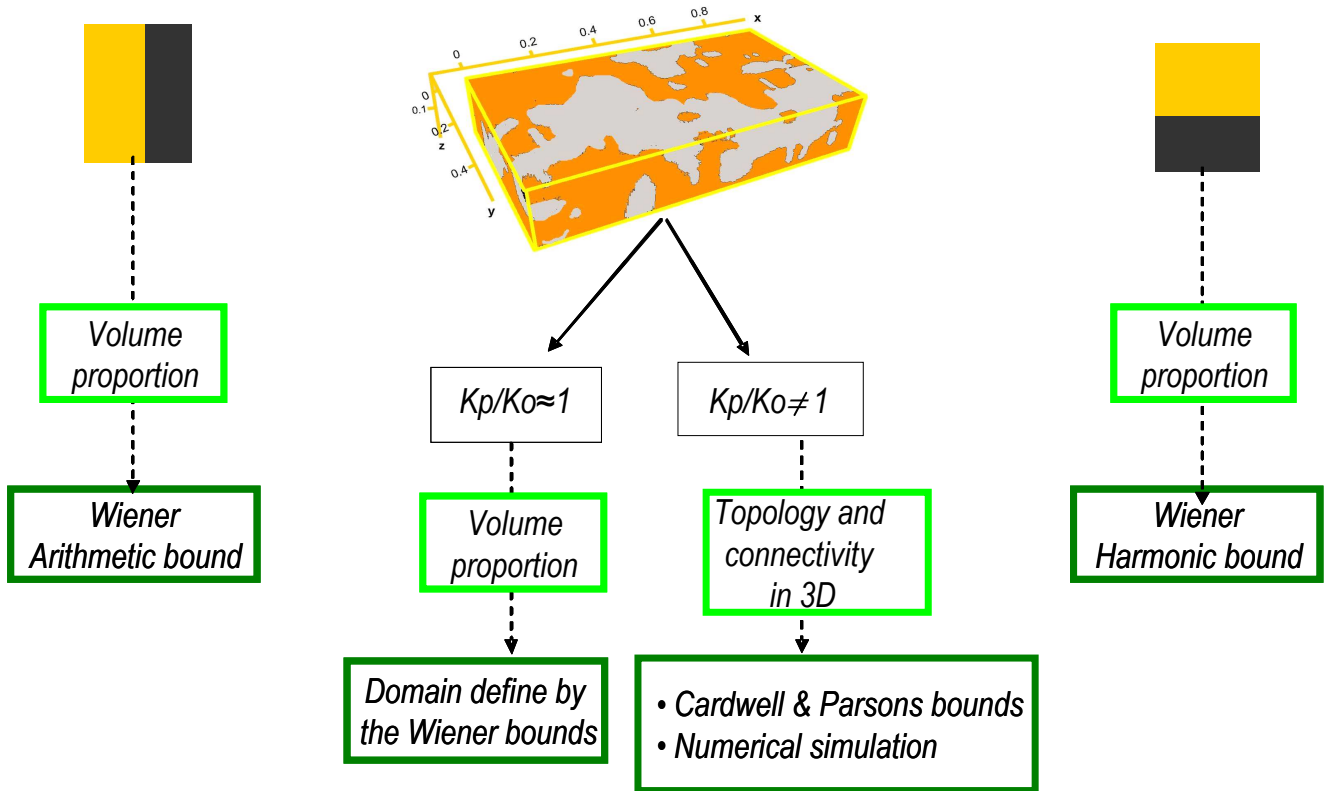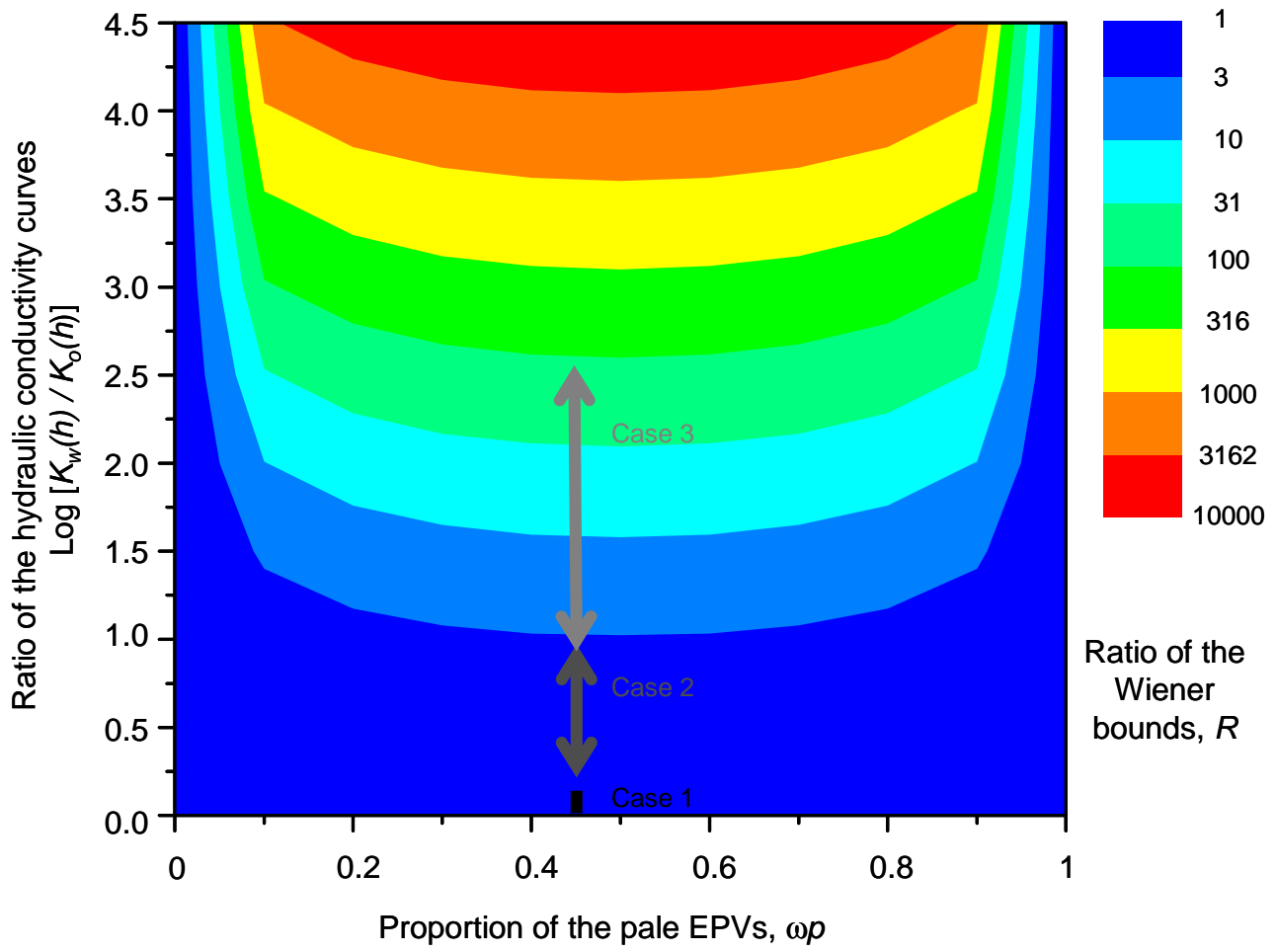
Figure 5

Figure 6

Depth (m)	Particle-size distribution (g kg^{-1})		
	< 2 µm	2 – 50 µm	50 – 2000 µm
0.35 – 0.45	182^p / 248°	714^p / 659°	104^p / 93°
0.45 – 0.55	213^p / 322°	706^p / 620°	81^p / 58°

.p: pale EPV
.o: ochre EPV   Table 1

	Nb (-)	Mean bulk density (g cm^3)	Mean saturated water content (cm^3 cm^{-3})	Coefficient of variation (%)
Pale EPV	15	1.53	0.423	2.76
Ochre EPV	18	1.57	0.408	3.75

Table 2

	case 1		case 2		case 3	
	pale	ochre	pale	ochre	pale	ochre
θ_s / cm^3 cm^{-3}	0,46	0,42	0,43	0,41	0,44	0,42
θ_r / cm^3 cm^{-3}	0,001	0,016	0,033	0,021	0,034	0,005
α / m^{-1}	0,23	1,64	0,55	1,21	0,72	0,66
n	1,33	1,15	1,23	1,13	1,16	1,15
K_s (m s^{-1})	1,40E-05	1,83E-06	1,98E-05	9,46E-06	1,64E-05	1,04E-05

Table 3

	S_{EPV}	S_{Wiener}	$S_{Cardwell-Pearson}$	$S_{Cardwell-Pearson}$ _ Numerical simulation		S_{Wiener} _ Numerical simulation	
				Upper Bound	Lower Bound	Upper Bound	Lower Bound
case 1	184,54	125,67	29,40	7,58	21,82	8,29	117,38
case 2	66,63	24,15	9,86	1,59	8,27	1,98	22,17
case 3	15,47	1,40	0,61	1,02	0,42	1,09	0,58

Table 4